Article

Facile Interfacial Engineering of Mesoporous TiO$_2$ for Low-Temperature Processed Perovskite Solar Cells

Jiyoon Nam [1,†], Inje Nam [1,†], Eun-Jin Song [2], Jung-Dae Kwon [2], Jongbok Kim [3], Chang Su Kim [2] and Sungjin Jo [1,*]

[1] School of Architectural, Civil, Environmental and Energy Engineering, Kyungpook National University, Daegu 41566, Korea

[2] Surface Technology Division, Korea Institute of Materials Science, 797 Changwondaero, Sungsan-Gu, Changwon, Gyeongnam 51508, Korea

[3] Department of Materials Science and Engineering, Kumoh National Institute of Technology, Gumi 39177, Korea

* Correspondence: sungjin@knu.ac.kr

† These authors contributed equally to this work.

check for updates

Abstract: The mesoporous TiO$_2$ nanoparticle-based scaffold structure is the best electron transport layer (ETL) for perovskite solar cells (PSCs) and is still used in most PSCs with optimal photovoltaic characteristics. However, the high sintering temperature of TiO$_2$ nanoparticles required to remove binders from the TiO$_2$ paste limits PSC application to flexible electronics. In this study, a simple interface modification process involving ethanol rinsing is developed to enhance the photovoltaic characteristics of low-temperature processed PSCs. This easy and fast technique could enable remarkable performance by PSCs by significantly increasing the fill factor and current density, leading to a power conversion efficiency more than four times that of untreated solar cells.

1. Introduction

Hybrid metal–halide perovskite solar cells (PSCs) have attracted considerable attention because of their low cost, high efficiency, and ease of fabrication. In addition to studies focused on their photovoltaic characteristics and the recent accomplishment of a power conversion efficiency (PCE) above 23% [1,2], research fields based on their flexible applications are also receiving much attention [3–5]. Conventional PSC fabrication methods, based on a solution process, are suitable for flexible polymer substrates [6,7]. However, the high-temperature sintering process that is required to remove organic binders and solvents from the TiO$_2$ paste used for the fabrication of the mesoporous TiO$_2$ electron transport layer (ETL) is not feasible for flexible polymer substrates. Hence, this high-temperature process limits the variety of substrates and the mass production scalability. To overcome these limitations, novel low-temperature processes and alternative materials for TiO$_2$ ETL fabrication have been investigated.

Mesoporous TiO$_2$ is still the best ETL for state-of-the-art PSCs [1,8–10]; the mesoporous scaffold structure is highly advantageous for electron transport since it increases the surface coverage between the TiO$_2$ nanoparticles and the perovskite light-absorbing layer [11]. Furthermore, the position of the conduction band minimum of TiO$_2$ is favorable for smooth electron transport from the light absorbing layer with a fast electron injection rate [12–14]. Nevertheless, studies on flexible PSCs based on mesoporous TiO$_2$ ETLs are scarce because of the abovementioned limitations. On the other hand, the substitution of mesoporous TiO$_2$ with low-temperature processable materials, such as [6,6]-phenyl-C$_{61}$-butyric acid methyl ester (PCBM), poly(3,4-ethylenedioxythiophene)–poly(styrene sulfonate) (PEDOT:PSS), ZnO,

Zn_2SnO_4, or Al_2O_3, is a common strategy to fabricate flexible PSCs [15–18]. However, the resulting photovoltaic characteristics are still inferior to those of mesoporous TiO_2-based devices. Several research groups have proposed different deposition methods for TiO_2 ETLs, including atomic layer deposition (ALD), electron beam deposition, and sputtering, to avoid the high-temperature sintering process. Still, all these techniques require some high-cost vacuum deposition equipment [19–21]. Low-temperature synthesis procedures for TiO_2 nanoparticles have also been reported [22,23]. However, the lower electron mobility and the creation of surface charge traps hinder the charge transport at the TiO_2/perovskite interface [24].

Here, we propose a facile interfacial engineering method to fabricate PSCs based on low-temperature sintered mesoporous TiO_2 (LT-PSCs). We developed a novel simple surface modification process (hereafter, SMP) that involves ethanol rinsing at the end of the mesoporous TiO_2 nanoparticles annealing; this SMP enhanced the PCE of the LT-PSCs more than four times compared with untreated PSCs. The proposed SMP has great scalability because it allows the use of conventional mesoporous TiO_2 ETLs at low temperatures. The reported findings herein could refine the current research direction for flexible PSCs.

2. Materials and Methods

2.1. Substrate Fabrication

A fluorine-doped tin oxide (FTO) substrate (Pilkington) was cleaned using a detergent, deionized water, acetone, and ethanol; then, its surface was pretreated via ultraviolet–ozone for 15 min. Titanium diisopropoxide bis(acetylacetonate) was diluted in 1-butanol to fabricate a blocking layer that was spin-coated on the FTO substrate and dried at 125 °C for 5 min. A TiO_2 nanoparticle paste (Greatcell Solar) was diluted in ethanol with a ratio of 1:10 (wt%) to obtain a mesoporous TiO_2 layer that was spin-coated on the FTO substrate under the same conditions as the blocking layer and sintered at various temperatures (from 150 to 550 °C) for 1 h. For the fabrication of multilayer (ML)-TiO_2, the TiO_2 nanoparticle paste was diluted in ethanol at a ratio of 1:30 (wt%). The LT-TiO_2-coated substrate was dipped in ethanol and stirred for 30 s after the mesoporous TiO_2 sintering to remove TiO_2 nanoparticle aggregates. The substrate was soaked in 20 mM aqueous $TiCl_4$ solution at 90 °C for 15 min. The cleaned substrates were sintered for 30 min under each condition.

2.2. PSC Fabrication

Methylammonium iodide (MAI), synthesized by reacting methylamine and hydriodic acid at 0 °C for 2 h, was rinsed with diethyl ether and dried in an oven at 80 °C for 24 h. PbI_2, MAI, dimethyl sulfoxide, and *N*,*N*-dimethylformamide were mixed to prepare a light-absorbing layer solution, which was spin-coated on the prepared substrate; diethyl ether was dripped on the center of the rotating substrate before the surface became hazed. An adduct solution-coated substrate was annealed first at 65 °C for 1 min and then at 100 °C for 10 min. To fabricate the hole transport layer, 2,2′,7,7′-tetrakis(*N*,*N*-di-*p*-methoxyphenylamine)-9,9′-spirobifluorene (Jilin), a lithium salt solution, 4-tert-butylpyridine, and chlorobenzene were mixed and the resulting solution was spin-coated on the $MAPbI_3$ layer. A silver electrode was deposited by using a thermal evaporator. All materials and chemicals were purchased from Sigma-Aldrich.

2.3. Measurements

The X-ray diffraction (XRD) spectra were recorded using a diffractometer (Bruker AXS, D8-Discover, Middlesex County, MA, USA) with a Cu X-ray tube in the 10–60° 2θ range. The photovoltaic characteristics were measured under air mass 1.5 G illumination (solar simulator, Model Sol2A, Oriel, Irvine, CA, USA) at 25 °C. Thermogravimetric analysis (TGA) was performed using a Q500 system (TA Instruments, New Castle, DE, USA) with an electronic scale during target combustion up to 600 °C. The surface profiles were characterized using a scanning electron microscope (SU8220, Hitachi, Tokyo, Japan).

3. Results and Discussion

Residual binders resulting from the insufficient sintering temperature of mesoporous TiO_2 paste are generally considered the reason for the degradation of the photovoltaic characteristics of PSCs [25] and, if they directly affect the solar cell properties, the crystallinity of the light-absorbing layer on TiO_2 ETL could also be potentially altered. Therefore, we investigated X-ray diffraction (XRD) patterns of the TiO_2 nanoparticles and the $CH_3NH_3PbI_3$ (MAPbI$_3$) light-absorbing layer at different TiO_2 sintering temperatures to monitor their crystallinity. Figure 1a shows the XRD pattern of TiO_2 nanoparticles at sintering temperatures between 150 and 550 °C; the diffraction peaks at 25.36°, 37.92°, and 54.82° correspond to the standard diffraction of the (101), (004), and (211) crystal planes, respectively, of anatase TiO_2 [26]. Regardless of the sintering temperature, these diffraction peaks are consistent with the standard anatase TiO_2 structure because commercial TiO_2 nanoparticles dispersed in organic binders and solvents have already been manufactured in the anatase structure. As regards the light-absorbing layer (Figure 1b), the peaks observed at 14.10°, 20.00°, 23.48°, 24.46°, 28.42°, 31.86°, 40.56°, and 43.12° correspond to the diffraction of the (110), (112), (211), (202), (220), (310), (224), and (314) crystal planes, respectively, of the conventional MAPbI$_3$ structure [27], and the spectra recorded at different sintering temperatures were consistent. Interestingly, these diffraction peaks did not exhibit any distinguishable phase singularity with the variation of the TiO_2 sintering temperature.
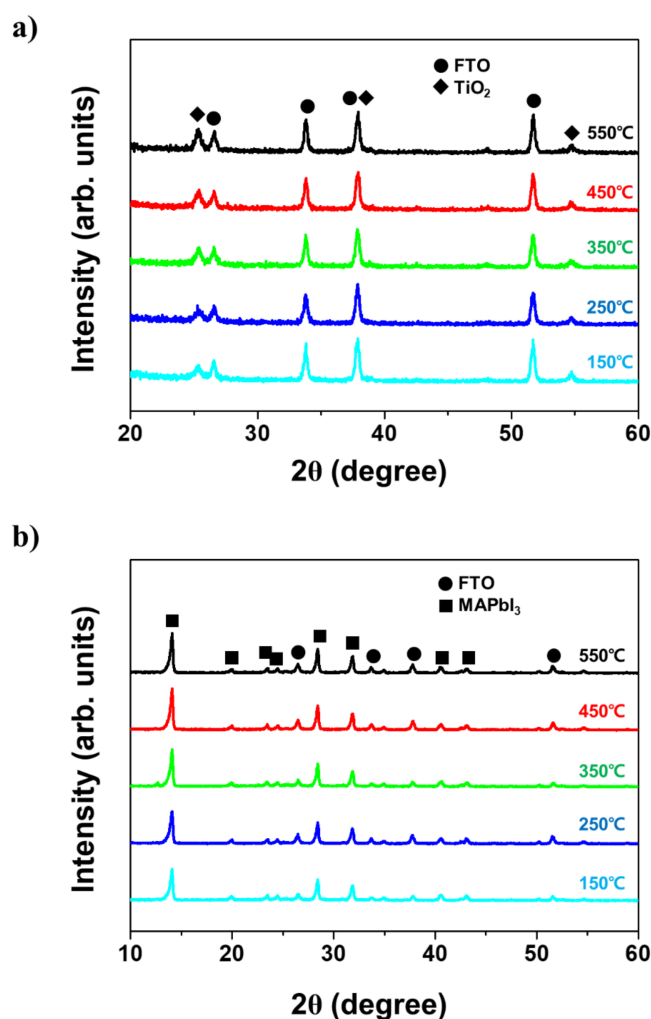
Figure 1. X-ray diffraction spectra of (**a**) mesoporous TiO_2 and (**b**) $CH_3NH_3PbI_3$ light-absorbing layers at various TiO_2 sintering temperatures.

However, previous studies on the sintering temperature of TiO_2 nanoparticles reported poor solar properties for PSCs fabricated at insufficient sintering temperatures [25]. We analyzed the photovoltaic characteristics of PSCs at different temperatures of mesoporous TiO_2 sintering to distinguish the consistency following the XRD results. Figure 2 shows the resulting current–voltage curves and histograms of photovoltaic characteristics; in contrast to the XRD data, the photovoltaic characteristics degraded as the TiO_2 sintering temperature decreased. In the 350–550 °C range, there was no significant change in the cell performance, but the photovoltaic characteristics worsened at 150 and 250 °C, indicating poor fill factor (FF) and current density (J_{sc}). The photovoltaic parameters of PSCs fabricated at various TiO_2 sintering temperatures are summarized in Table 1. The J_{sc}, open-circuit voltage (V_{oc}), FF, and PCE values for the high sintering temperature (550 °C) were 20.61 mA/cm^2, 1.01 V, 0.66, and 13.67%, respectively. The PCE did not significantly degrade even when the sintering temperature was lowered to 350 °C, while J_{sc} and FF began to decrease at temperatures below 250 °C, resulting in a significantly poorer PCE (1.85%).
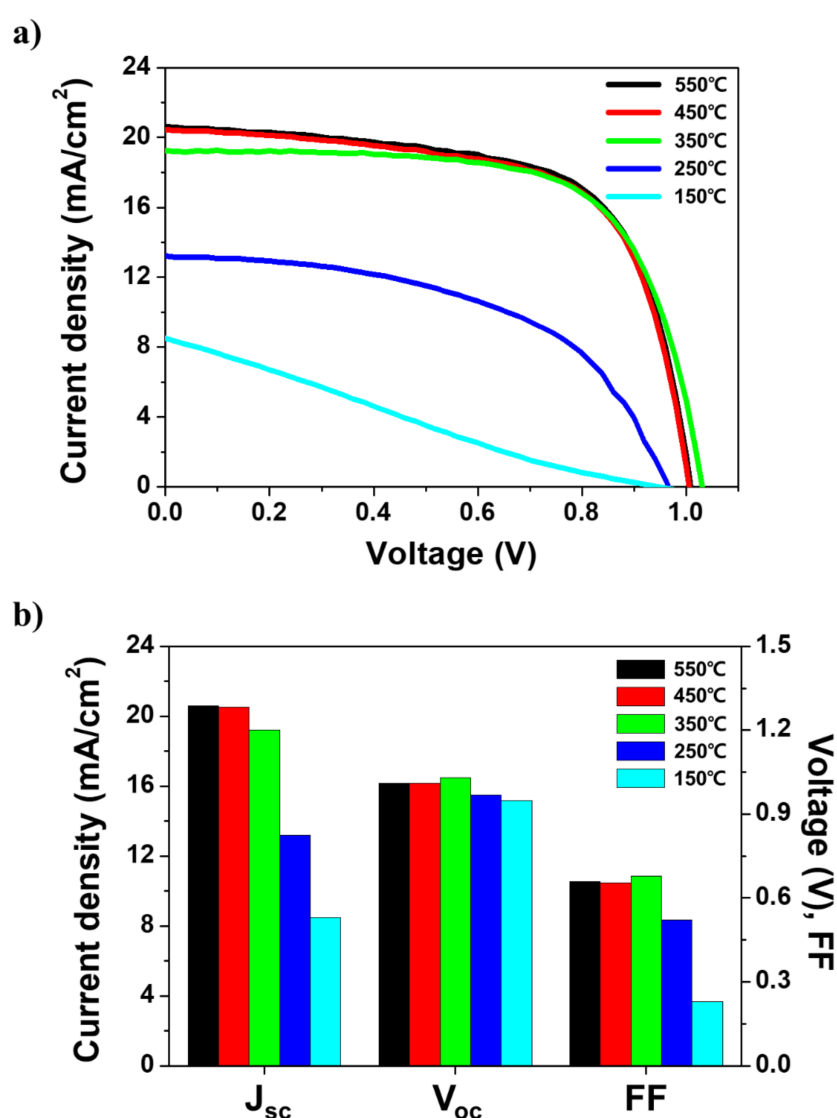

Figure 2. (**a**) Current–voltage curves and (**b**) variations in the current density (J_{sc}), open-circuit voltage (V_{oc}), and fill factor (FF) of perovskite solar cells based on mesoporous TiO_2 sintered at different temperatures.

Table 1. Photovoltaic parameters (current density (J_{sc}), open-circuit voltage (V_{oc}), fill factor (FF), and power conversion efficiency (PCE)) for perovskite solar cells based on mesoporous TiO_2 sintered at different temperatures, with and without the surface modification process (SMP).

| TiO_2 Sintering Temperature (°C)	J_{sc} (mA/cm^2)	V_{oc} (V)	FF	PCE (%)
550	20.61	1.01	0.66	13.67
450	20.46	1.01	0.65	13.49
350	19.23	1.03	0.68	13.45
250	13.20	0.97	0.52	6.63
150 (without SMP)	8.50	0.95	0.23	1.85
150 (with SMP)	13.86	1.00	0.60	8.27

Despite the discordance between the solar performances estimated based on the TiO_2 sintering temperature trend and the consistency of the XRD results, the data shown in Figure 2 indicate quite clearly the presence of certain decline points among the sintering temperatures tested. Figures 1 and 2 demonstrate that other dominant factors affected the photovoltaic characteristics. Therefore, we assume that the mesoporous TiO_2/MAPbI$_3$ interface was responsible for the degradation of the photovoltaic characteristics when decreasing the sintering temperature.

Mesoporous TiO_2 nanoparticles are generally sintered at high temperatures to remove organic binders and evaporate solvents. Since the carbonaceous residues need to be combusted at temperatures above 300 °C, the TiO_2 sintering was conducted at 400–500 °C in most previous studies [28]. We carried out a thermogravimetric analysis (TGA) to determine the cascading tendency and verify the exact combustion or evaporation points of the binder components. TGA is usually used to identify the thermal behavior of target materials by measuring the weight of the residuals after the heating process. Figure 3 shows the temperature–weight curve for the TiO_2 paste after annealing at 600 °C, revealing several distinct weight loss points around 100 and 300 °C. Many previous TGA studies on TiO_2 nanoparticles have suggested various thermal behaviors for the TiO_2 paste components [25,29]. In our data, the first weight loss at ~100 °C corresponds to the volatilization of organic solvents, which was complete at ~200 °C; the organic binders, mostly ethyl cellulose, were combusted between 200 and 300 °C, representing the second weight loss. In other words, the ETL sintered at a relatively low temperature had residues on the TiO_2 nanoparticle surface and such interfacial impurities between the TiO_2 ETL and MAPbI$_3$ layer might have hindered the charge transport system. The small weight loss at a high sintering temperature (above 300 °C) was due to the combustion of the few carbonaceous residuals from the organic binders. Based on the TGA data, we assume that the degraded properties of the LT-PSCs were due to the insufficient organic binder combustion and solvent evaporation, which resulted in the interfacial impurities between the TiO_2 ETL and MAPbI$_3$ layer.
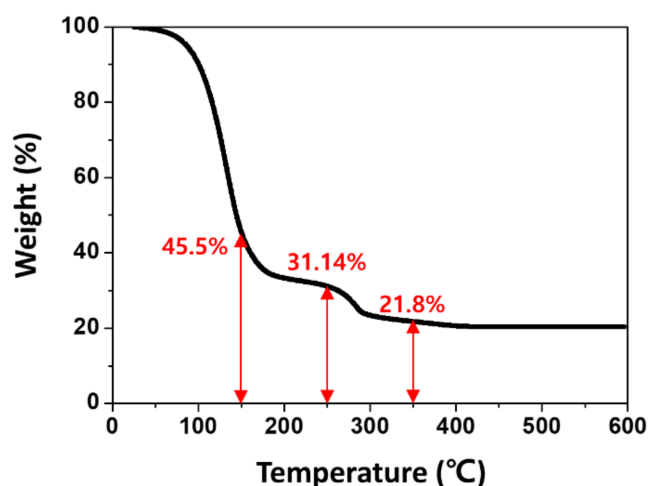
Figure 3. Thermogravimetric analysis curve of TiO_2 nanoparticle paste.

Therefore, we tried to identify other dominant factors affecting the TiO_2 ETL surface and degrading the photovoltaic characteristics of the fabricated LT-PSCs. In our experiments, the surface coating uniformity of the $MAPbI_3$ layer on the LT-TiO_2 was inferior to that on PSCs based on high-temperature sintered mesoporous TiO_2. The poor morphology of the $MAPbI_3$ surface could be observed even with the naked eye; therefore, we collected scanning electron microscopy (SEM) images of the TiO_2 ETL surface to microscopically determine the dominant degradation factors. Figure 4a,b displays the SEM images of the mesoporous TiO_2 layer sintered at 150 °C without SMP, showing a typical surface profile of mesoporous scaffold at low magnification (20,000×), but also showing visible agglomerates (TiO_2 nanoparticles and carbonaceous materials) at high magnification (100,000×). During $TiCl_4$ dipping, which is an essential chemical treatment used to enhance the surface roughness and necking of mesoporous TiO_2 [30], the agglomerates assembled on the TiO_2 scaffold. These agglomerates are believed to hinder the formation of a uniform $MAPbI_3$ layer and worsen, as interfacial defects, the surface coverage between the TiO_2 ETL and $MAPbI_3$ layer, disturbing the charge transport. Therefore, we infer that the low PCE of the fabricated LT-PSCs was caused by the presence of such agglomerates on the ETL surface. Hence, the photovoltaic characteristics should be boosted by their removal. To obtain a uniform surface of the mesoporous TiO_2 layer, it was dipped in ethanol and stirred for 30 s after sintering at low temperature; without any further treatment, the agglomerates were entirely removed through this simple SMP (Figure 4c,d).
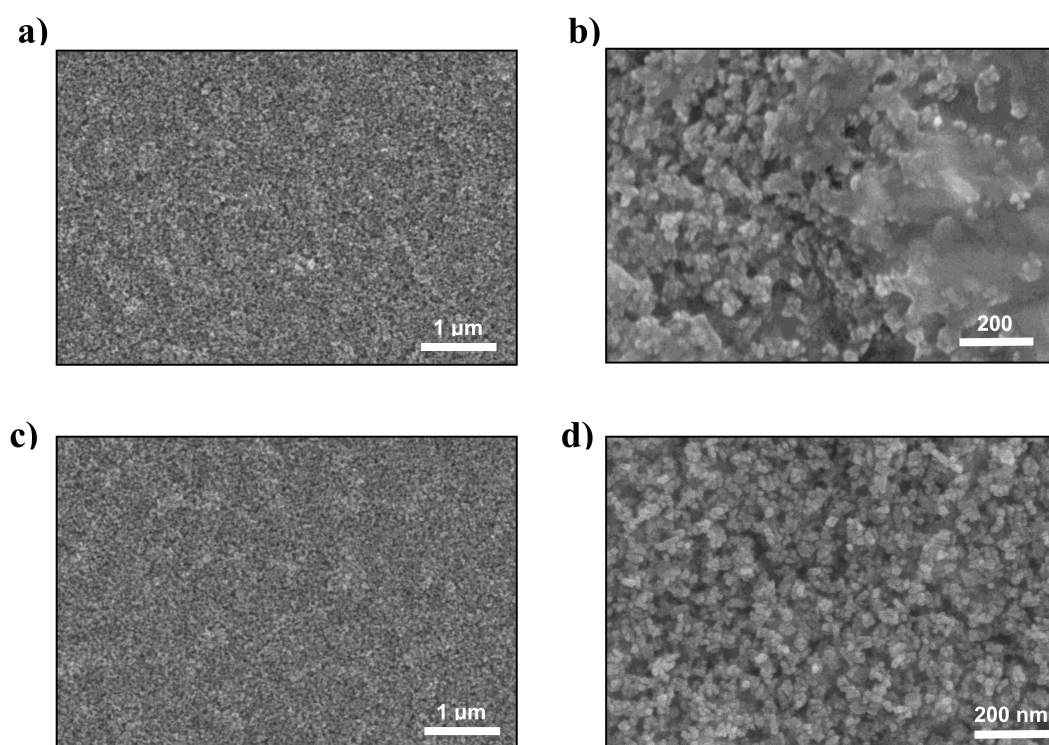
Figure 4. Scanning electron microscopy images of mesoporous TiO_2 sintered at low temperatures (**a**,**b**) without and (**c**,**d**) with the surface modification process, at (**a**,**c**) 20,000× and (**b**,**d**) 100,000× magnification.

To clarify the effectiveness of the proposed SMP, we fabricated other LT-PSCs in the same way, in addition to treating them via the SMP after the mesoporous TiO_2 sintering at 150 °C. First, we conducted the SMP with various rinsing solvents to determine the change in the photovoltaic characteristics based on the use of different rinsing solvents such as ethanol, acetone, isopropyl alcohol (IPA), and deionized water (DI). As shown in Figure S1, solvents other than ethanol exhibited poor photovoltaic performance. It is assumed that the SMP with ethanol is the most effective method for removing the surface agglomerates because ethanol is used as the solvent for the dissolution of TiO_2

paste to fabricate the mesoporous TiO_2 ETL. Figure 5 compares the photovoltaic characteristics of LT-PSCs realized with and without the SMP, showing that most parameters, including the J_{sc}, V_{oc}, and FF, were significantly improved by the SMP (Table 1). The PCE (8.27%) was increased more than four times compared to that achieved without the SMP (1.85%), and it even exceeded that of the PSCs based on TiO_2 sintered at 250 °C (6.63%). These results imply that the proposed SMP could enable a facile interfacial modification of low-temperature sintered TiO_2 layers, greatly enhancing the PCE of LT-PSCs.
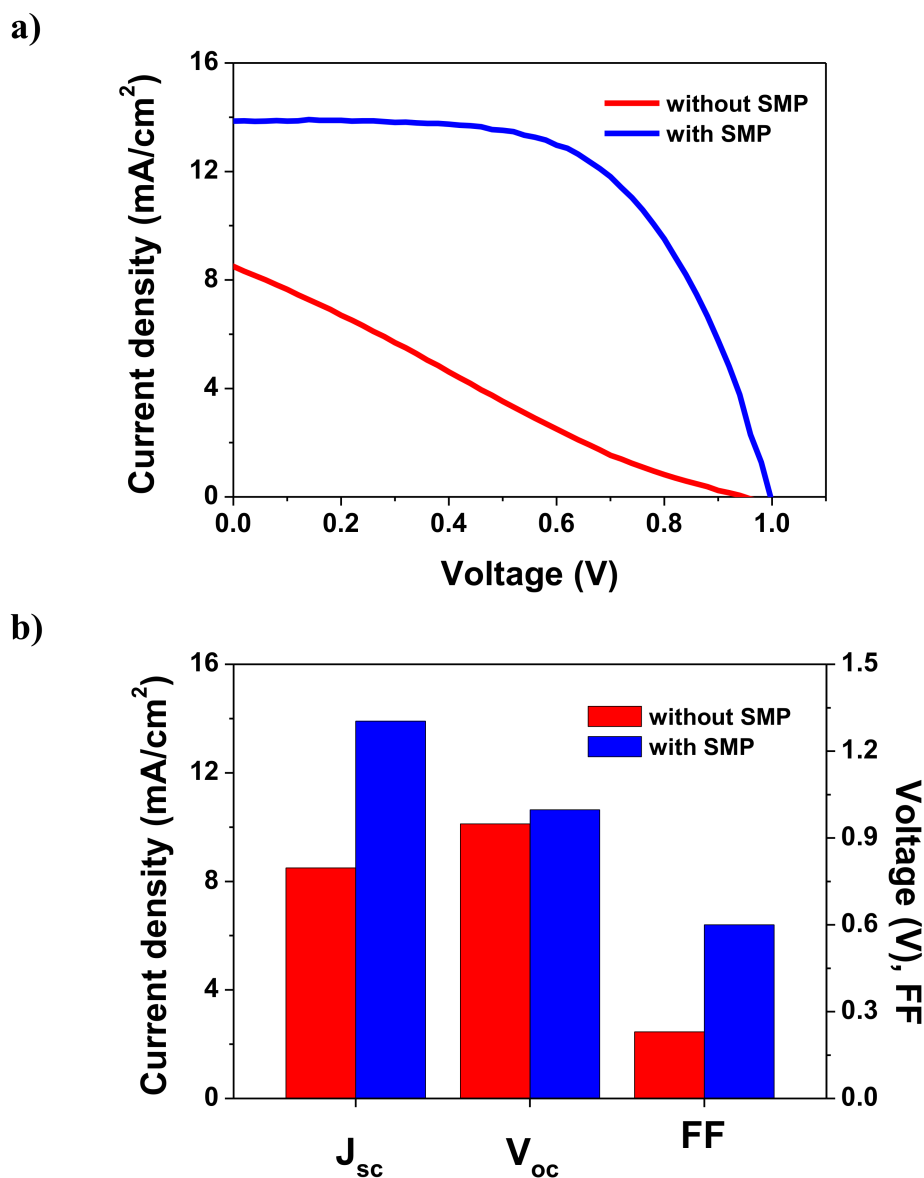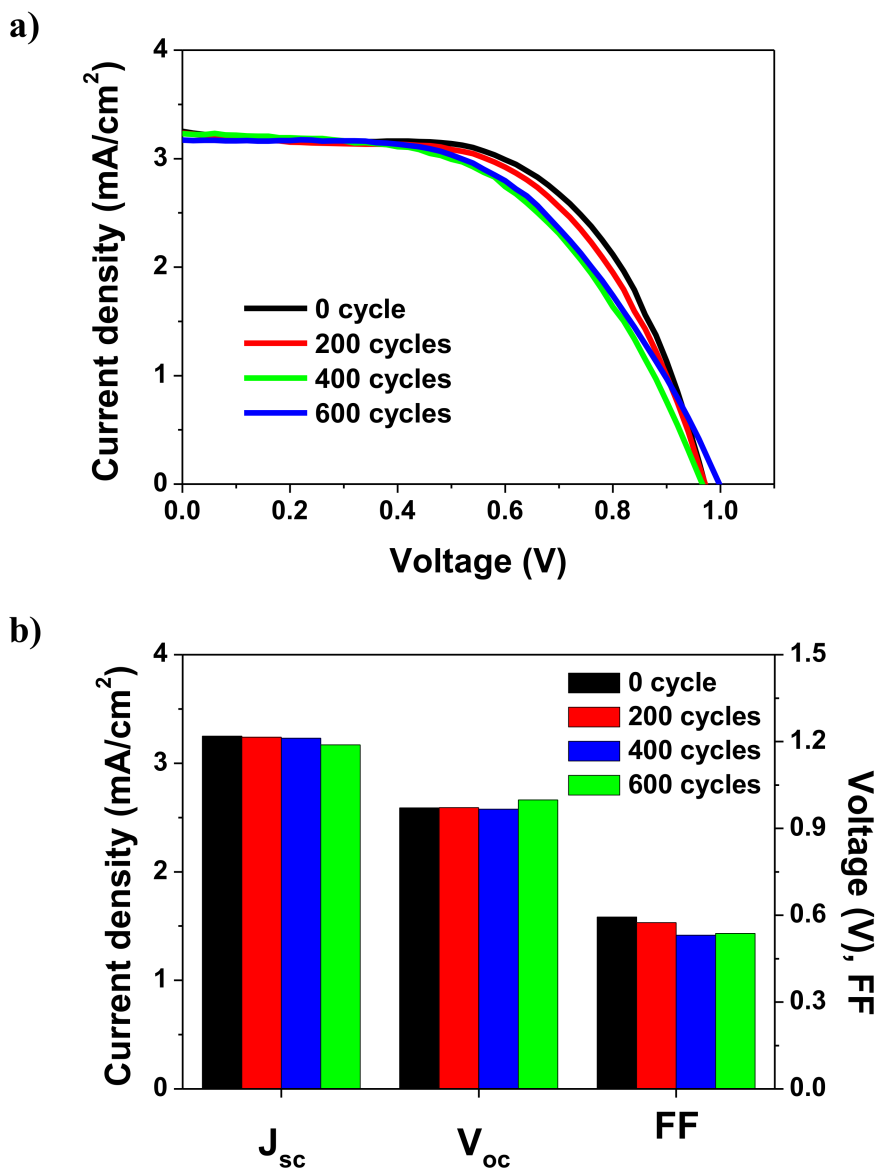

Figure 5. (**a**) Current–voltage curves and (**b**) current density (J_{sc}), open-circuit voltage (V_{oc}), and fill factor (FF) values of perovskite solar cells based on mesoporous TiO_2 sintered at a low temperature, with and without the surface modification process (SMP).

A multiple SMP was also developed to maximize the interface modification effect; one-third thickness of mesoporous TiO_2 was coated and followed by SMP, and these two steps were repeated three times to complete the TiO_2 ETL fabrication. Figure S2 shows the SEM images of the LT-TiO_2 after a single SMP and the individual layers of multilayer TiO_2 (ML-TiO_2) with the SMP from the first to third layers, respectively. There were no distinguishable differences on the surface of each layer for the ML-TiO_2 compared with the single layer of LT-TiO_2. This corroborates the utility of the SMP, even in

multiple coating processes of mesoporous TiO_2. Furthermore, multiple iterations of the SMP improved the photovoltaic characteristics of the PSCs compared to those treated via a single SMP (Figure S3).

Finally, we successfully fabricated LT-PSCs via the SMP on a polyethylene naphthalate (PEN)/indium tin oxide (ITO) flexible substrate. The advantage of the SMP including the low-temperature process is that it facilitates the simple fabrication of flexible PSCs directly on a polymer substrate, without any substitution of the mesoporous TiO_2 ETL. Figure 6 shows the resulting photovoltaic characteristics; these flexible LT-PSCs exhibited stable performance during the bending test at a bending radius of 10 mm.

Figure 6. (**a**) Current–voltage curves and (**b**) variations in the current density (J_{sc}), open-circuit voltage (V_{oc}), and fill factor (FF) of flexible perovskite solar cells based on mesoporous TiO_2 sintered at a low temperature and fabricated on a polyethylene naphthalate film, as functions of the bending cycles.

4. Conclusions

The novel and simple SMP proposed in this study for LT-PSCs significantly enhanced their photovoltaic characteristics using the conventional mesoporous TiO_2 ETL. By eliminating the agglomerates on the mesoporous TiO_2 surface, this method guarantees a uniform and dense light-absorbing layer during the manufacturing process. The effective manufacturing of LT-PSCs

was demonstrated by applying the SMP to the surface of a mesoporous TiO_2 ETL. Significant improvements of the photovoltaic characteristics were observed. Moreover, the best ETL for PSCs and a low-temperature process could be used simultaneously. This brief and easy method to fabricate advanced LT-PSCs will benefit future developments for flexible, bendable, large-scale, and printable applications. Our ongoing research includes follow-up studies to enhance the advantages of the SMP and develop additional effective surface treatments.

Supplementary Materials: The following are available online at http://www.mdpi.com/2079-4991/9/9/1220/s1, Figure S1: SEM images of the surfaces of single and multilayer TiO_2, Figure S2: Current–voltage curves and photovoltaic characteristics of perovskite solar cells based on single and multilayer TiO_2.

Author Contributions: S.J. conceived and designed the research. E.-J.S. and J.-D.K. participated in the fabrication of the thin film of TiO_2 on PEN substrates. J.N. and I.N. participated in materials preparation, device fabrication, and data interpretation. S.J. and J.N. wrote the paper. S.J. supervised the project. All authors discussed the results and commented on the manuscript.

Conflicts of Interest: The authors declare no conflict of interest.

References

1. Green, M.A.; Dunlop, E.D.; Levi, D.H.; Hohl-Ebinger, J.; Yoshita, M.; Ho-Baillie, A.W. Solar cell efficiency tables (version 54). *Prog. Photovolt.* **2019**, *27*, 565–575. [CrossRef]
2. Jung, E.H.; Jeon, N.J.; Park, E.Y.; Moon, C.S.; Shin, T.J.; Yang, T.-Y.; Noh, J.H.; Seo, J. Efficient, stable and scalable perovskite solar cells using poly(3-hexylthiophene). *Nature* **2019**, *567*, 511–515. [CrossRef] [PubMed]
3. Giacomo, F.D.; Zardetto, V.; D'Epifanio, A.; Pescetelli, S.; Matteocci, F.; Razza, S.; Di Carlo, A.; Licoccia, S.; Kessels, W.M.M.; Creatore, M.; et al. Flexible perovskite photovoltaic modules and solar cells based on atomic layer deposited compact layers and UV-irradiated TiO_2 scaffolds on plastic substrates. *Adv. Energy Mater.* **2015**, *5*, 1401808. [CrossRef]
4. Zhou, Y.Q.; Wu, B.S.; Lin, G.H.; Xing, Z.; Li, S.H.; Deng, L.L.; Chen, D.C.; Yun, D.Q.; Xie, S.Y. Interfacing pristine C_{60} onto TiO_2 for viable flexibility in perovskite solar cells by a low-temperature all-solution process. *Adv. Energy Mater.* **2018**, *8*, 1800399. [CrossRef]
5. Najafi, M.; Giacomo, F.D.; Zhang, D.; Shanmugam, S.; Senes, A.; Verhees, W.; Hadipour, A.; Galagan, Y.; Aernouts, T.; Veenstra, S.; et al. Highly efficient stable flexible perovskite solar cells with metal oxides nanoparticle charge extraction layers. *Small* **2018**, *14*, 1702775. [CrossRef] [PubMed]
6. Dkhissi, Y.; Meyer, S.; Chen, D.; Weerasinghe, H.C.; Spiccia, L.; Cheng, Y.B.; Caruso, R.A. Stability comparison of perovskite solar cells based on zinc oxide an titania on polymer substrates. *ChemSusChem* **2016**, *9*, 687–695. [CrossRef] [PubMed]
7. Guo, Y.; Sato, W.; Shoyama, K.; Nakamura, E. Sulfamic acid-catalyzed lead perovskite formation for solar cell fabrication on glass or plastic substrates. *J. Am. Chem. Soc.* **2016**, *138*, 5410–5416. [CrossRef] [PubMed]
8. Yang, W.S.; Park, B.W.; Jung, E.H.; Jeon, N.J.; Kim, Y.C.; Lee, D.U.; Shin, S.S.; Seo, J.; Kim, E.K.; Noh, J.H.; et al. Iodide management in formamidinium-lead-halide–based perovskite layers for efficient solar cells. *Science* **2017**, *356*, 1376–1379. [CrossRef]
9. Jung, E.H.; Jeon, N.J.; Park, E.Y.; Moon, C.S.; Shin, T.J.; Yang, T.Y.; Noh, J.H.; Seo, J. Efficient, stable and scalable perovskite solar cells using poly(3-hexylthiophene). *Nature* **2019**, *567*, 511–516. [CrossRef]
10. Yang, W.S.; Noh, J.H.; Jeon, N.J.; Kim, Y.C.; Ryu, S.; Seo, J.; Seok, S.I. High-performance photovoltaic perovskite layers fabricated through intramolecular exchange. *Science* **2015**, *348*, 1234–1237. [CrossRef]
11. Lee, M.M.; Teuscher, J.; Miyasaka, T.; Murakami, T.N.; Snaith, H.J. Efficient hybrid solar cells based on meso-superstructured organometal halide perovskites. *Science* **2012**, *338*, 643–647. [CrossRef] [PubMed]
12. Mahmood, K.; Sarwar, S.; Mehran, M.T. Current status of electron transport layers in perovskite solar cells: Materials and properties. *RSC Adv.* **2017**, *7*, 17044. [CrossRef]
13. Yang, G.; Tao, H.; Qin, P.; Ke, W.; Fang, G. Recent progress in electron transport layers for efficient perovskite solar cells. *J. Mater. Chem. A* **2016**, *4*, 3970. [CrossRef]

14. Huwang, X.; Hu, Z.; Xu, J.; Wang, P.; Wang, L.; Zhang, J.; Zhu, Y. Low-temperature processed SnO_2 compact layer by incorporating TiO_2 layer toward efficient planar heterojunction perovskite solar cells. *Sol. Energy Mater. Sol. Cells* **2017**, *164*, 87–92. [CrossRef]

15. Zhang, J.; Tan, C.H.; Du, T.; Morbidoni, M.; Lin, C.T.; Xu, S.; Durrant, J.R.; McLachlan, M.A. ZnO-PCBM bilayers as electron transport layers in low-temperature processed perovskite solar cells. *Sci. Bull.* **2018**, *63*, 343–348. [CrossRef]

16. You, J.; Hong, Z.; Yang, Y.; Chen, Q.; Cai, M.; Song, T.B.; Chen, C.C.; Lu, S.; Liu, Y.; Zhou, H.; et al. Low-temperature solution-processed perovskite solar cells with high efficiency and flexibility. *ACS Nano* **2014**, *8*, 1674–1680. [CrossRef] [PubMed]

17. Shin, S.S.; Yang, W.S.; Noh, J.H.; Suk, J.H.; Jeon, N.J.; Park, J.H.; Kim, J.S.; Seong, W.M.; Seok, S.I. High-performance flexible perovskite solar cells exploiting Zn_2SnO_4 prepared in solution below 100 °C. *Nat. Commun.* **2015**, *6*, 7410. [CrossRef]

18. Ball, J.M.; Lee, M.M.; Hey, A.; Snaith, H.J. Low-temperature processed meso-superstructured to thin-film perovskite solar cells. *Energy Environ. Sci.* **2013**, *6*, 1739–1743. [CrossRef]

19. Kim, B.J.; Kim, D.H.; Lee, Y.Y.; Shin, H.W.; Han, G.S.; Hong, J.S.; Mahmood, K.; Ahn, T.K.; Joo, Y.C.; Hong, K.S.; et al. Highly efficient and bending durable perovskite solar cells: Toward a wearable power source. *Energy Environ. Sci.* **2015**, *8*, 916–921. [CrossRef]

20. Hossain, M.; Naka, S.; Okada, H. Annealing effect of E-beam evaporated TiO_2 films and their performance in perovskite solar cells. *J. Photochem. Photobiol. A* **2018**, *360*, 109–116. [CrossRef]

21. Yang, D.; Yang, R.; Zhang, J.; Yang, Z.; Liu, S.F.; Li, C. High efficiency flexible perovskite solar cells using superior low temperature TiO_2. *Energy Environ. Sci.* **2015**, *8*, 3208–3214. [CrossRef]

22. Rao, A.R.; Dutta, V. Low-temperature synthesis of TiO_2 nanoparticles and preparation of TiO_2 thin films by spray deposition. *Sol. Energy Mater. Sol. Cells.* **2007**, *91*, 1075–1080.

23. Conings, B.; Baeten, L.; Jacobs, T.; Dera, R.; D'Haen, J.; Manca, J.; Boyen, H.G. An easy-to-fabricate low-temperature TiO_2 electron collection layer for high efficiency planar heterojunction perovskite solar cells. *APL Mater.* **2014**, *2*, 081505. [CrossRef]

24. Wali, Q.; Iqbal, Y.; Pal, B.; Lowe, A.; Jose, R. Tin oxide as an emerging electron transport medium in perovskite solar cells. *Sol. Energy Mater. Sol. Cells.* **2018**, *179*, 102–117. [CrossRef]

25. Holliman, P.J.; Muslem, D.K.; Jones, E.W.; Connell, A.; Davies, M.L.; Charbonneau, C.; Carnie, M.J.; Worsley, D.A. Low temperature sintering of binder-containing TiO_2/metal peroxide pastes for dye-sensitized solar cells. *J. Mater. Chem. A* **2014**, *2*, 11134–11143. [CrossRef]

26. Che, M.; Zhu, L.; Zhao, Y.L.; Yao, D.S.; Gu, X.O.; Song, J.; Qiang, Y.H. Enhancing current density of perovskite solar cells using TiO_2-ZrO_2 composite scaffold layer. *Mater. Sci. Semicond. Process.* **2016**, *56*, 29–36. [CrossRef]

27. Jiang, M.; Wu, J.; Lan, F.; Tao, Q.; Gao, D.; Li, G. Enhancing the performance of planar organo-lead halide perovskite solar cells by using a mixed halide source. *J. Mater. Chem. A* **2015**, *3*, 963–967. [CrossRef]

28. Nakazaki, J.; Segawa, H. Evolution of organometal halide solar cells. *J. Photochem. Photobiol. C* **2018**, *35*, 74–107. [CrossRef]

29. Lin, J.; Nattestad, A.; Yu, H.; Bai, Y.; Wang, L.; Dou, S.X.; Kim, J.H. Highly connected hierarchical textured TiO_2 spheres as photoanodes for dye-sensitized solar cells. *J. Mater. Chem. A* **2014**, *2*, 8902–8909. [CrossRef]

30. Ito, S.; Murakami, T.N.; Comte, P.; Liska, P.; Grätzel, C.; Nazeeruddin, M.K.; Grätzel, M. Fabrication of thin film dye sensitized solar cells with sola to electric power conversion efficiency over 10%. *Thin Solid Films* **2008**, *516*, 4613–4619. [CrossRef]